Theor. Comput. Fluid Dyn. (2007) 21: 1–13
DOI 10.1007/s00162-006-0037-7

ORIGINAL ARTICLE

E. Leriche · G. Labrosse

Vector potential–vorticity relationship for the Stokes flows: application to the Stokes eigenmodes in 2D/3D closed domain

Received: 2 December 2005 / Accepted: 18 July 2006 / Published online: 5 October 2006

Abstract The unsteady dynamics of the Stokes flows, where $\vec{\nabla}^2\left(\frac{p}{\rho}\right) = 0$, is shown to verify the vector potential–vorticity ($\vec{\psi}$, $\vec{\omega}$) correlation $\frac{\partial\vec{\psi}}{\partial t} + \nu\,\vec{\omega} + \vec{\Pi} = 0$, where the field $\vec{\Pi}$ is the pressure-gradient vector potential defined by $\vec{\nabla}\left(\frac{p}{\rho}\right) = \vec{\nabla}\times\vec{\Pi}$. This correlation is analyzed for the Stokes eigenmodes, $\frac{\partial\vec{\psi}}{\partial t} = \lambda\,\vec{\psi}$, subjected to no-slip boundary conditions on any two-dimensional (2D) closed contour or three-dimensional (3D) surface. It is established that an asymptotic linear relationship appears, verified in the core part of the domain, between the vector potential and vorticity, $\nu\,(\vec{\omega} - \vec{\omega}_0) = -\lambda\,\vec{\psi}$, where $\vec{\omega}_0$ is a constant offset field, possibly zero.

Keywords Stokes flow · Stokes eigenmodes

PACS 47.10-g, 4715G-

1 Introduction

Incompressible flows ($\vec{\nabla}\cdot\vec{\mathbf{v}} = 0$) can be equivalently described by the vector potential $\vec{\psi}$ from which they can be derived ($\vec{\mathbf{v}} = \vec{\nabla}\times\vec{\psi}$). Its determination (up to the gradient of any harmonic function, and verifying the constraint $\vec{\nabla}\cdot\vec{\psi} = 0$) is made possible by the existence of the right number of boundary conditions [7]. For planar flows, the vector potential reduces to a one-component vector along the normal to the flow plane. This component is the stream function, ψ. The same simplification occurs for the vorticity $\vec{\omega} = \vec{\nabla}\times\vec{\mathbf{v}}$, where ω denotes its unique component, along the normal to the flow plane as well, for planar flows.

Both $\vec{\psi}$ and $\vec{\omega}$ are pseudo-vectors, that is they transform themselves in the opposite way with respect to the proper vectors in a mirror reflection operation. The vorticity is not specifically related to incompressible

Communicated by T. Colonius

E. Leriche (✉)
Laboratoire d'Ingénierie Numérique, Institut des Sciences de l'Energie, Faculté des Sciences et Techniques de l'Ingénieur, Ecole Polytechnique Fédérale de Lausanne, Station 9, 1015 Ecublens, Switzerland
E-mail: emmanuel.leriche@epfl.ch

G. Labrosse
Department of Chemical Engineering, University of Florida 227 ChE,
PO Box 116005, Gainesville, FL 32611, USA

G. Labrosse
Université Paris-Sud, Limsi-CNRS Bat. 508, 91405 Orsay Cedex, France
E-mail: labrosse@limsi.fr

flow, in contrast to the vector potential. Therefore, any incompressible flow is characterized by two separately defined pseudo-vectors, differing however in one important aspect: the vorticity is completely defined whilst the vector potential is defined up to the gradient of an harmonic function. Would it be that they are functionally related, but associated with a third pseudo-vector whose role is to compensate for the arbitrariness of $\vec{\psi}$? The answer is positive for the Stokes flows, with a relation $\frac{\partial \vec{\psi}}{\partial t} + \nu\, \vec{\omega} + \vec{\Pi} = 0$ involving a pressure-gradient vector potential, $\vec{\Pi}$, defined by $\vec{\nabla}\left(\frac{p}{\rho}\right) = \vec{\nabla} \times \vec{\Pi}$. This ensures that the pressure verifies the harmonicity relation, $\vec{\nabla}^2\left(\frac{p}{\rho}\right) = 0$. This $(\vec{\psi}, \vec{\omega})$ relationship contains all the dynamics of these flows. As for $\vec{\psi}$ and $\vec{\omega}$, for planar flows the pressure-gradient vector potential reduces to a one-component vector along the normal to the flow plane. This component is named the pressure-gradient potential, Π.

The fundamental question of a possible vector potential–vorticity $(\vec{\psi},\ \vec{\omega})$ relationship was initially raised by Batchelor in a 1956 paper [1], but only for the two-dimensional (2D) inviscid (large Reynolds number) steady laminar flows whose stream lines are closed. Expressing this relation is still an open question. Correlation $\omega(\psi)$ models, such as $\omega \propto \sinh(\beta\psi)$, are in particular associated with statistical-mechanical description of decaying 2D turbulence (see [17] and references therein).

Later, Batchelor [2] again conjectured the existence of a relationship between ψ and ω, but regarding the 2D viscous flows (zero Reynolds number), writing "Thus a solution for ψ as a function of x and y obtained from $-\omega = \Delta\psi = \lambda\psi$ represents either a steady motion of an inviscid fluid, or, when multiplied by $\exp(-\lambda t)$, a decaying motion of viscous fluid.".

More recently, a scattered $(\psi,\ \omega)$ correlation was provided in [15,16] for five Stokes eigenmodes in the square. A detailed presentation of the Stokes eigenspace in the square is now available in [9]. Its most interesting feature is that the eigenmodes dynamics behave as if they were isobaric in the square core denoted therein by $\mathcal{R}_C$ and arbitrarily defined to be $[-0.6, +0.6]^2$, for a $[-1, +1]^2$ square domain. Within $\mathcal{R}_C$, each eigenmode is shown to verify the simple $\omega \propto -\lambda\psi$ relationship, where λ is the associated Stokes eigenvalue. This is a nice confirmation of the conjecture opened by Batchelor about the viscous flows.

In the present paper, a general exact vectorial $(\vec{\psi},\ \vec{\omega})$ relation is settled for any unsteady Stokes flow. Then, guided by the analysis made in [9], this relation is applied to the Stokes eigenmodes confined in the disk, in the plane channel, in the square and in the cube. It is shown that, in the core of these domains, and therefore of any closed 2D or 3D domain, these modes verify the linear relationship $\vec{\omega} - \vec{\omega}_0 = -\left(\frac{\lambda}{\nu}\right)\ \vec{\psi}$, where $\vec{\omega}_0$ is a constant, possibly zero, offset field.

2 Stokes problems

2.1 Stokes problem formulations

Let the unsteady Stokes velocity and total pressure fields, $(\vec{\mathbf{v}},\ p)$, be solutions of

$$\begin{aligned}
\tfrac{\partial \vec{\mathbf{v}}}{\partial t} &= \nu\, \vec{\nabla}^{\mathbf{2}}\vec{\mathbf{v}} - \vec{\nabla}\left(\tfrac{p}{\rho}\right) && \text{for } \mathbf{x} \in \Omega,\ \ t > 0,\\
\vec{\nabla} \cdot \vec{\mathbf{v}} &= 0 && \text{for } \mathbf{x} \in \Omega,\ \ t > 0,\\
\vec{\mathbf{v}} &= \vec{\mathbf{V}}(\mathbf{x}, \mathbf{t}) && \text{for } \mathbf{x} \in \partial\Omega,\ \ t > 0,\\
\vec{\mathbf{v}}(\mathbf{x}, t = 0) &= \vec{\mathbf{V}}_{\mathbf{0}}(\mathbf{x}) && \text{for } \mathbf{x} \in \Omega,
\end{aligned} \tag{1}$$

where ν is the momentum diffusivity, ρ is the constant fluid density, Ω is the open domain and $\partial\Omega$ its closure. $\vec{\mathbf{V}}(\mathbf{x}, \mathbf{t})$ and $\vec{\mathbf{V}}_{\mathbf{0}}(\mathbf{x})$ are compatible velocity fields. The $\frac{p}{\rho}$ field can contain any source term that derives from a scalar potential, such as, for instance, the gravity or a centrifugal acceleration. The first two equations of (1) imply that the pressure verifies

$$\vec{\nabla}^{\mathbf{2}}\left(\frac{p}{\rho}\right) = 0, \quad \text{for } \mathbf{x} \in \Omega,\ \ t > 0. \tag{2}$$

This is the key relation of this analysis. The pressure $\frac{p}{\rho}$ is said to be harmonic. It cannot be periodic along all the space directions, unless constant, and, if it is periodic along one (or two) directions, it has to monotonically decrease along the remaining normal direction. Equation (2) leads to consider on the same level the velocity and pressure gradient as both deriving from a vector potential:

$$\vec{\mathbf{v}} = \vec{\nabla} \times \vec{\psi}, \quad \vec{\nabla}\left(\frac{p}{\rho}\right) = \vec{\nabla} \times \vec{\Pi}, \quad \text{for } \mathbf{x} \in \Omega, \ t > 0. \tag{3}$$

The $\vec{\psi}$ and $\vec{\Pi}$ fields are subjected to analogous determination constraints, namely

$$\vec{\nabla} \cdot \vec{\psi} = 0 = \vec{\nabla} \cdot \vec{\Pi}, \quad \text{for } \mathbf{x} \in \Omega, \ t > 0, \tag{4}$$

together with the additional specific kinematic relations:

$$\vec{\omega} = -\vec{\nabla}^2 \vec{\psi}, \quad \vec{\nabla}^2 \vec{\Pi} = 0, \quad \text{for } \mathbf{x} \in \Omega, \ t > 0\,. \tag{5}$$

Both fields are defined up to an additive arbitrary constant vectorial field.

2.2 Stokes eigenproblem

The Stokes eigenmodes $(\vec{\mathbf{v}}, p)$ are defined by

$$\begin{array}{rl} \lambda\, \vec{\mathbf{v}} = \nu\, \vec{\nabla}^{\mathbf{2}} \vec{\mathbf{v}} - \vec{\nabla}\left(\frac{p}{\rho}\right) & \text{for } \mathbf{x} \in \Omega, \\ \vec{\nabla} \cdot \vec{\mathbf{v}} = 0 & \text{for } \mathbf{x} \in \Omega, \\ \vec{\mathbf{v}} = \mathbf{0} & \text{for } \mathbf{x} \in \partial\Omega, \end{array} \tag{6}$$

where the eigenvalues λ are strictly negative [5, 14]. An alternative form of the system (6) is its vector potential formulation, with $\vec{\psi}$ verifying

$$\left(\lambda - \nu\, \vec{\nabla}^{\mathbf{2}}\right) \vec{\nabla}^{\mathbf{2}} \vec{\psi} = 0 \quad \text{for } \mathbf{x} \in \Omega\,, \tag{7}$$

$$\vec{\nabla} \cdot \vec{\psi} = 0 \quad \text{for } \mathbf{x} \in \Omega\,, \tag{8}$$

together with homogeneous no-slip/no-flux boundary conditions [7]:

$$\vec{\psi} = \frac{\partial \vec{\psi}}{\partial n} = 0 \quad \text{for } \mathbf{x} \in \partial\Omega \quad , \tag{9}$$

where n is the coordinate evaluated along $\vec{\mathbf{n}}$, the unit vector normal to $\partial\Omega$.

3 Stokes flow dynamics

3.1 General relation for unsteady flows

Let us write down the generic relation which characterizes the solutions of (1)–(5). To this end we consider any surface S, delimited by a closed contour C, and crossed by the flow whose net local volumetric flux per second is

$$\int\limits_{(S)} \frac{\partial \vec{\mathbf{v}}}{\partial t} \cdot \mathrm{d}\vec{\mathbf{S}} = \int\limits_{(C)} \frac{\partial \vec{\psi}}{\partial t} \cdot \mathrm{d}\vec{\mathbf{l}}. \tag{10}$$

By the first equation of (1) this flux is also given by

$$\int\limits_{(S)} \frac{\partial \vec{\mathbf{v}}}{\partial t} \cdot \mathrm{d}\vec{\mathbf{S}} = \int\limits_{(S)} \left(\nu\, \vec{\nabla}^{\mathbf{2}} \vec{\mathbf{v}} - \vec{\nabla}\left(\frac{p}{\rho}\right)\right) \cdot \mathrm{d}\vec{\mathbf{S}}. \tag{11}$$

The first r.h.s. term is easily transformed, using the incompressibility constraint, to become the vorticity circulation along C, namely

$$\int\limits_{(S)} \vec{\nabla}^2 \vec{\mathbf{v}} \cdot \mathrm{d}\vec{\mathbf{S}} = -\int\limits_{(S)} \vec{\nabla} \times \vec{\omega} \cdot \mathrm{d}\vec{\mathbf{S}} = -\int\limits_{(C)} \vec{\omega} \cdot \mathrm{d}\vec{\mathbf{l}}. \tag{12}$$

The pressure gradient flux through $\mathrm{d}\vec{\mathbf{S}}$ also leads, via the pressure-gradient vector potential $\vec{\Pi}$ introduced by Eq. (3), to a contour integral:

$$\int\limits_{(S)} \vec{\nabla}\left(\frac{p}{\rho}\right) \cdot \mathrm{d}\vec{\mathbf{S}} = \int\limits_{(C)} \vec{\Pi} \cdot \mathrm{d}\vec{\mathbf{l}}. \tag{13}$$

From Eq. (11), taking into consideration that Eqs. (10,12,13) imply an arbitrary closed contour C, the local differential relationship follows:

$$\frac{\partial \vec{\psi}}{\partial t} + \nu\,\vec{\omega} + \vec{\Pi} = 0, \quad \text{for } \mathbf{x} \in \Omega\ ,\ t > 0\ . \tag{14}$$

3.2 Steady Stokes flows

In this case, the relation (14) simplifies to

$$\nu\,\vec{\omega} + \vec{\Pi} = 0\ , \quad \text{for } \mathbf{x}\ \in \Omega\ .$$

As a matter of a first illustration of $\vec{\Pi}$ for this kind of flow, let us consider the steady $(\hat{\mathbf{e}}_x, \hat{\mathbf{e}}_y)$-plane Poiseuille flow given by $\vec{\mathbf{v}} = U\left(1 - \left(\frac{y}{H}\right)^2\right)\hat{\mathbf{e}}_x$ and $\vec{\nabla}\left(\frac{p}{\rho}\right) = G\hat{\mathbf{e}}_x$, with U a velocity scale and G a constant pressure gradient, related by $G = -\frac{2\nu U}{H^2}$. Both $\nu\,\vec{\omega}$ and $\vec{\Pi}$ have only one component, normal to the flow plane, that is along $\hat{\mathbf{e}}_z$, given by $\pm Gy$, respectively, as expected.

3.3 Stokes eigenmodes

Applying this relation to a Stokes eigenmode verifying Eq. (6) yields the local algebraic relationship

$$\lambda\vec{\psi} + \nu\,\vec{\omega} + \vec{\Pi} = 0\ , \quad \text{for } \mathbf{x} \in \Omega\ . \tag{15}$$

A systematic analysis of the consequences of this general vectorial relation is provided in the next sections. It leads, through the introduction of the $\vec{\Pi}$ field, to a full understanding of the already published scalar relationships $(\psi,\ \omega)$ in the square [9,15,16].

4 Stokes eigenmodes dynamics

This section aims to illustrate and interpret the relation (15), with, in particular, a first use of the $\vec{\Pi}$ vector potential. Three cases which can be analytically handled, the fully space-periodic Stokes eigenmodes and those defined in a disk and in a plane channel, are considered. They are taken as a guide to prepare the analysis of the numerically computed $(\vec{\psi},\ \vec{\omega})$ relationship obtained for Stokes eigenmodes that cannot be analytically determined, such as in squared or cubical domains. This section ends with a generalization of the analysis results to the Stokes eigenmodes dynamics in any closed domain.

4.1 Fully space-periodic Stokes eigenmodes

The fully space-periodic Stokes eigenmodes, those that are not constrained to verify any boundary conditions, are well known. First, by harmonicity of the pressure, they are isobaric, that is such that $\vec{\nabla}\left(\frac{p}{\rho}\right) = 0$ everywhere. To be periodic in all the space directions, the pressure can only be constant. Correlatively, these eigenmodes satisfy exactly the functional relationship $\nu\,\vec{\omega} = -\lambda\,\vec{\psi}$ everywhere, thanks to the fact that the vector potential $\vec{\psi}$ is not subjected to vanish on any closed contour (2D case) or surface (3D case).

4.2 Stokes eigenmodes in the disk and plane channel

4.2.1 Stokes eigenmodes in the disk

In a disk of unit radius with $\phi \in [0, 2\pi[$, the stream function $\psi(r, \phi)$ and the pressure $p(r, \phi)$ are given by

$$\psi(r, \phi) = \left[J_m\left(\sqrt{-\lambda/\nu}\, r\right) - J_m\left(\sqrt{-\lambda/\nu}\right)\, r^m \right] e^{im\phi}, \tag{16}$$

$$\frac{p(r, \phi)}{\rho} = \mathrm{i}\lambda J_m\left(\sqrt{-\lambda/\nu}\right)\, r^m \mathrm{e}^{\mathrm{i}m\phi}, \tag{17}$$

where m must be an integer ($m = 0, \ldots, \infty$) because the fundamental wavelength is fixed to 2π, and J_m is a Bessel function of the first kind. $\sqrt{-\lambda/\nu}$ are the roots of

$$\sqrt{-\lambda/\nu}\; J'_m\left(\sqrt{-\lambda/\nu}\right) = m\; J_m\left(\sqrt{-\lambda/\nu}\right).$$

These roots are of infinite number for each m. The vorticity ω is thus given by

$$\nu\, \omega(r, \phi) = -\lambda\; J_m\left(\sqrt{-\lambda/\nu}\, r\right) \mathrm{e}^{\mathrm{i}m\phi} = -\lambda \left[\psi(r, \phi) + J_m\left(\sqrt{-\lambda/\nu}\right)\, r^m \mathrm{e}^{\mathrm{i}m\phi} \right]. \tag{18}$$

This relation gives the expression for Π, the only nonzero component of $\vec{\Pi}$, $\vec{\Pi} = \Pi(r, \phi)\, \hat{\mathbf{e}}_z$,

$$\Pi(r, \phi) = \lambda\; J_m\left(\sqrt{-\lambda/\nu}\right)\, r^m \mathrm{e}^{\mathrm{i}m\phi}, \tag{19}$$

as can be checked using the definition (3) of $\vec{\Pi}$. For subsequent use, let us write this component in the case $m = 0$. It is constant:

$$\Pi_{m=0}(r, \phi) = \lambda\; J_0\left(\sqrt{-\lambda/\nu}\right). \tag{20}$$

4.2.2 Stokes eigenmodes in the plane channel

The one-dimensional confined (in $x \in [-1, +1]$) Stokes eigenmodes are presented in detail in [12]. They are expressed according to

$$\begin{pmatrix} \mathbf{u} \\ p \end{pmatrix} = \begin{pmatrix} \tilde{\mathbf{u}}(x) \\ \tilde{p}(x) \end{pmatrix} \mathrm{e}^{\mathrm{i}my + \lambda t},$$

where $(\tilde{\mathbf{u}}(x),\ \tilde{p}(x))$ are complex functions and m is any real number, since, contrary to the disk case, there is no fundamental wavelength in the channel. The associated stream functions can be cast into two parts, each one of given symmetry with x, the symmetric being denoted by $\psi_{\mathrm{e}}(x, y)$, and the antisymmetric by $\psi_{\mathrm{o}}(x, y)$. Their expressions are given by

$$\psi_{\mathrm{e}}(x, y) = \left(\frac{\cosh(mx)}{\cosh(m)} - \frac{\cos(\mu_{\mathrm{e}} x)}{\cos(\mu_{\mathrm{e}})} \right) \sin(my),$$

$$\psi_{\mathrm{o}}(x, y) = \left(\frac{\sinh(mx)}{\sinh(m)} - \frac{\sin(\mu_{\mathrm{o}} x)}{\sin(\mu_{\mathrm{o}})} \right) \cos(my)\ .$$

The corresponding eigenvalues $\lambda = -\nu\,(m^2 + \mu^2)$ are obtained by imposing that their normal flux should cancel on the boundary, $x = \pm 1$. This leads to transcendental relations in μ_{e} or μ_{o},

$$\mu_{\mathrm{e}}\, \tan(\mu_{\mathrm{e}}) = -m\, \tanh(m), \quad \mu_{\mathrm{o}}\, \cot(\mu_{\mathrm{o}}) = m\, \coth(m)\ .$$

The first eigenvalues are listed in [12] for $m = 1, 10$. The corresponding vorticities are then

$$\nu\, \omega_{\mathrm{e}}(x, y) = \lambda\, \frac{\cos(\mu_{\mathrm{e}} x)}{\cos(\mu_{\mathrm{e}})}\, \sin(my) = -\lambda \left(\psi_{\mathrm{e}}(x, y) - \frac{\cosh(mx)}{\cosh(m)}\, \sin(my) \right) \tag{21}$$

$$\nu\, \omega_{\mathrm{o}}(x, y) = \lambda\, \frac{\sin(\mu_{\mathrm{o}} x)}{\sin(\mu_{\mathrm{o}})}\, \cos(my)\ = -\lambda \left(\psi_{\mathrm{o}}(x, y) - \frac{\sinh(mx)}{\sinh(m)}\, \cos(my) \right). \tag{22}$$

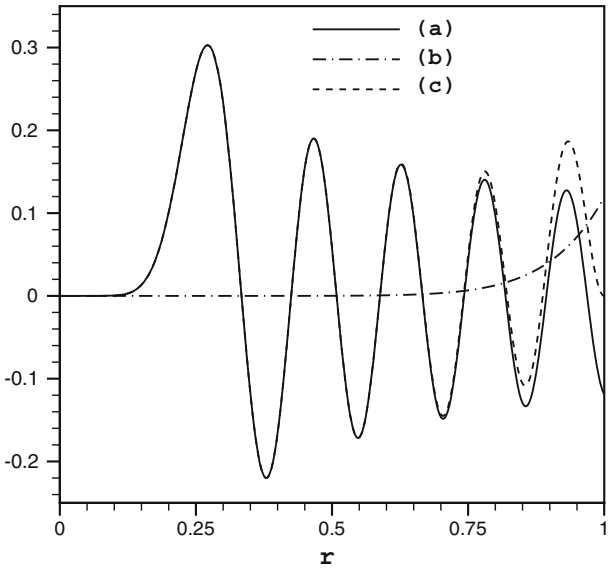

Fig. 1 **a** $\left(-\frac{\nu}{\lambda}\right)\omega(r, \phi = 0)$, **b** $-\frac{1}{\lambda}\Pi(r, \phi = 0)$ and **c** $\psi(r, \phi = 0)$ for the $(m = 10, \sqrt{-\lambda/\nu} = 43.368)$ disk eigenmode

Here again, one directly gets the expression of Π_e and Π_o, the only nonzero components of $\vec{\Pi}_e$ and $\vec{\Pi}_o$, $\vec{\Pi}_{\substack{e\\o}} = \Pi_{\substack{e\\o}}(x, y)\,\hat{\mathbf{e}}_z$, with

$$\Pi_e(x, y) = -\lambda\,\frac{\cosh(mx)}{\cosh(m)}\,\sin(my) \tag{23}$$

and

$$\Pi_o(x, y) = -\lambda\,\frac{\sinh(mx)}{\sinh(m)}\cos(my), \tag{24}$$

as can be checked using the $\vec{\Pi}$ definition relation (3).

4.2.3 Analysis

The stream function–vorticity $(\psi,\ \omega)$ relationships (18), (21), (22) exhibit a deep analogy. Let us describe the behavior of the functions $\Pi = -(\nu\,\omega + \lambda\psi)$. They are periodic, like ψ and ω, with m as a wavenumber along the direction tangential to the boundary. The stream function is imposed to be an arbitrary constant on the boundary, a constant usually chosen to be zero, in contrast with the vorticity which has no prescribed value there. Balancing the boundary value of ω, according to $\left(\frac{\nu\omega+\Pi}{-\lambda}\right) = \psi$, is made possible by the presence of Π. This is illustrated, in the disk and channel (even-mode) cases, with the 10th eigenmode of $m = 10$ respectively computed for $\phi = 0$ and $y = \frac{\pi}{2m}$. Figures 1 and 2 show the functions $-\frac{\nu\omega}{\lambda}$, $-\frac{\Pi}{\lambda}$ and ψ, respectively, for $\sqrt{-\lambda/\nu} = 43.368$ and 32.7740 ($\mu = 31.2111$ for the channel mode). The effect of the $-\frac{\Pi}{\lambda}$ and ψ boundary compensation is obvious, but $-\frac{\Pi}{\lambda}$ damps progressively into the domain from the boundary, as shown by the $-\frac{\Pi}{\lambda}$ function in curves (b) of Figs. 1 and 2; this damping becomes increasingly pronounced as m increases, in the disk and the channel, as given by Eqs. (19), (23), and (24).

4.2.4 The $(\psi,\ \omega)$ relationship in the disk

Let us start with the axisymmetric eigenmodes in the disk, $m = 0$. They of course satisfy the exact relationship

$$\lambda\psi + \nu\,\omega + \Pi_{m=0} = 0\,, \quad \text{for } r \in [0, 1],\ \forall\,\phi, \tag{25}$$

with $\Pi_{m=0}$ given by (20). This linear relationship between ψ and ω exhibits a constant offset, $\Pi_{m=0}$, which gives ω a constant value, noted ω_0, at each radial location where ψ cancels. The Stokes eigenvalue λ governs

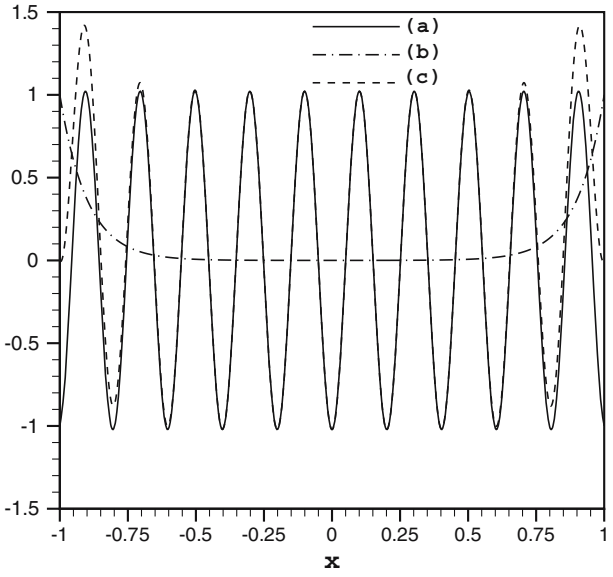

Fig. 2 **a** $\left(-\frac{\nu}{\lambda}\right)\omega(x,\, y=\frac{\pi}{2m})$, **b** $-\frac{1}{\lambda}\Pi(x,\, y=\frac{\pi}{2m})$ and **c** $\psi(x,\, y=\frac{\pi}{2m})$ for the ($m=10$, $\mu=31.2111$) channel eigenmode

the number of the radial zeroes of ψ, as well as the ω_0 value. In this particular case, the exact (ψ, ω) linear relationship is

$$\lambda\psi + \nu\ (\omega - \omega_0(\lambda)) = 0\ , \quad \text{for } r \in [0,\, 1],\ \ \forall\phi,$$

with $\nu\,\omega_0(\lambda) = -\lambda\ J_0\left(\sqrt{-\lambda/\nu}\right)$.

Let us follow the same approach to describe the (ψ, ω) relationships associated with the non-axisymmetric eigenmodes. The only difference comes from the fact that the offset is now a function of r and ϕ, $\Pi(r,\phi)$ as given by Eq. (19). The ϕ dependence factorizes in the general relation

$$\lambda\psi(r,\phi) + \nu\,\omega(r,\phi) + \Pi(r,\phi) = 0\ , \quad \text{for } r \in [0,\, 1] \times \phi \in [0,\, 2\pi[, \tag{26}$$

and can be discarded from the discussion.

The left part of Fig. 3 shows a (ψ, ω) scatter plot made from the disk eigenmode depicted in Fig. 1. The plot contains 1,001 values of $\left(-\frac{\nu}{\lambda}\right)\omega(r,\,\phi=0)$ and $\psi(r,\,\phi=0)$ obtained on a uniform meshing of $r \in [0,\, 1]$. The characteristic locations of this correlation plot are the zeroes of $\psi(r,\,\phi=0)$ listed in Table 1. At all these locations, we have $\left(-\frac{\nu}{\lambda}\right)\omega(r,\,\phi=0) = \frac{\Pi(r,\phi=0)}{\lambda}$, with $\Pi(r,\,\phi=0)$ decreasing monotonically from the boundary toward the center of the disk. Reading the correlation plot is made easy by following the way each arc [curve (c) in Fig. 1] joining two successive zeroes of $\psi(r,\,\phi=0)$ transforms in the (ψ, ω) plot.

For instance, the first arc, between $r=1$ and $r=0.89$, leads to the first curved branch of this scatter plot, with $\left(-\frac{\nu}{\lambda}\right)\omega(r,\,\phi=0)$ going from -0.12 to -0.036. The same occurs with the next arcs, but each time with less effect from $\Pi(r,\,\phi=0)$, which leads to a stacking up of the curved branches onto a limit straight-line branch, like that presented in the right part of Fig. 3. This plot only contains the data corresponding to $r \in [0,\, 0.75]$, that is the internal region of the disk wherein $\Pi(r,\,\phi=0)$ gets very small (see Table 1). This limit branch still possesses a structure whose amplitude is so small that this branch can be practically described by the average relation $\nu\,\omega = -\lambda\,\psi$. Here, no offset comes into this relation, since $\Pi(r,\,\phi)$ vanishes for $r \to 0$. The reference [9], dedicated to the Stokes eigenmodes in the square, introduced $\mathcal{R}_C$ for denoting the core part of the confined domain where this simple (ψ, ω) relationship holds. In the other region of the flow, denoted by $\mathcal{R}_B$, the $\frac{\Pi}{\lambda}$ contribution is essential for the previously mentioned boundary compensation. This occurs in a layer going along the boundaries, whose thickness decreases with m.

4.2.5 The (ψ, ω) relationship in the plane channel

The (ψ, ω) correlation plot (not shown) of the plane channel case is similar to that of the disk case. The previous description also holds, but with a slight modification in the x-symmetric $\psi_e(x,\, y)$ situation. Indeed, an

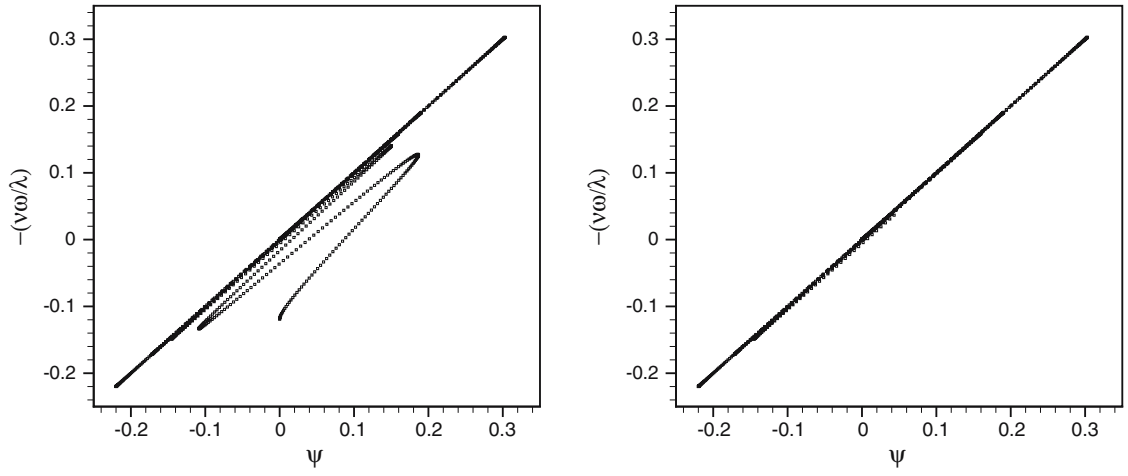

Fig. 3 Scatter plot of values of $\left(-\frac{\nu}{\lambda}\right)\omega(r, \phi = 0)$ and $\psi(r, \phi = 0)$ for the ($m = 10$, $\sqrt{-\lambda/\nu} = 43.368$) disk eigenmode; *(left)* 1,001 values in $r \in [0, 1]$, *(right)* 751 values in $r \in [0, 0.75]$

Table 1 Radial locations of the zeros of $\psi(r, \phi = 0)$ and the corresponding values taken by $-100\,\frac{\Pi(r,\phi=0)}{\lambda}$

r	0	0.33	0.43	0.51	0.59	0.67	0.74	0.82	0.89	1
$-100\,\frac{\Pi(r)}{\lambda}$	0	2.0×10^{-4}	0.002	0.014	0.06	0.21	0.6	1.7	3.6	12

offset is present in the core of the domain, $|x| \to 0$, and the linear relationship reads $\nu\ (\omega - \omega_0(y)) = -\lambda\,\psi$, where, according to Eq. (23), $\nu\,\omega_0(y) = -\Pi_e(x \to 0, y) = -\lambda\,\frac{\sin(my)}{\cosh(m)}$. This offset is modulated in y, but with an amplitude that decreases exponentially with m.

4.3 The Stokes eigenmodes in the square

These Stokes eigenmodes are not accessible by analytical means, but can only be determined by numerical tools [10]. Two eigenmodes of the square are chosen in order to show that they exhibit the same behavior as those of the disk and plane channel eigenmodes. They are noted $E1$, ($\lambda/\nu = -13.086172791$), and $E2$, ($\lambda/\nu = -331.966266$), where $E1$ is the fundamental mode presented in [9,13].

For each eigenmode, a figure (Fig. 4 for $E1$ and Fig. 5 for $E2$) shows contours in the (x, y) plane of $\left(-\frac{\nu}{\lambda}\right)\omega(x, y)$ in (a), $\psi(x, y)$ in (b) and $\frac{\Pi(x,y)}{(-\lambda)}$ in (c), *with the same scales and levels* in these three plots. Plots (c) of Figs. 4 and 5 clearly show that the $\frac{\Pi(x,y)}{(-\lambda)}$ fields of $E1$ and $E2$ have a quasi-periodic behavior along the boundary and an exponential decrease of their amplitude moving into the domain from the boundary. This supplies a way of quantitatively comparing the plots (a) and (b) of the same figures, and completes the comment made in Sect. 8.2.2 of [9].

Figure 6 gives the functions $\left(-\frac{\nu}{\lambda}\right)\omega(x, y = y_0)$, $\psi(x, y = y_0)$ and $\frac{\Pi(x,y=y_0)}{(-\lambda)}$, with $y_0 = 0$ for $E1$ and $y_0 = -0.259$ for $E2$. They should be compared to those given in Fig. 2, except that, for reasons of symmetry, the $E2$ curves are odd with x, giving the functional $\frac{\Pi(x,y=y_0)}{(-\lambda)}$ a $\sinh(mx)$ shape, instead of the $\cosh(mx)$ present in Fig. 2. It should be noticed that the hyperbolic decrease of $\frac{\Pi(x,y=y_0)}{(-\lambda)}$ with x is almost as pronounced for the fundamental $E1$ and $E2$ eigenmodes. As expected, these modes mainly differ by the number of internal zeroes of the $\psi(x, y = y_0)$ functions.

A third set of figures is proposed for each of the $E1$ and $E2$ modes, Figs. 7 and 8, respectively. Each figure contains three scatter plots, based on 97^2 Chebyshev nodal values distributed in the square, of $(\psi,\ \omega)$ correlations respectively obtained: (a) along the line $y = y_0$, (b) in the whole square and (c) in the internal part of the square, $\mathcal{R}_C = (x, y) \in [-0.6, 0.6]^2$. The parts (a) confirm the description made of the left chart of Fig. 3. There is no internal zero of the $E1$'s $\psi(x, y = y_0)$ function (Fig. 6), and therefore no arc in the corresponding $(\psi,\ \omega)$ correlation scatter plot [chart (a) of Fig. 7], while $E2$'s $\psi(x, y = y_0)$ function (Fig. 6)

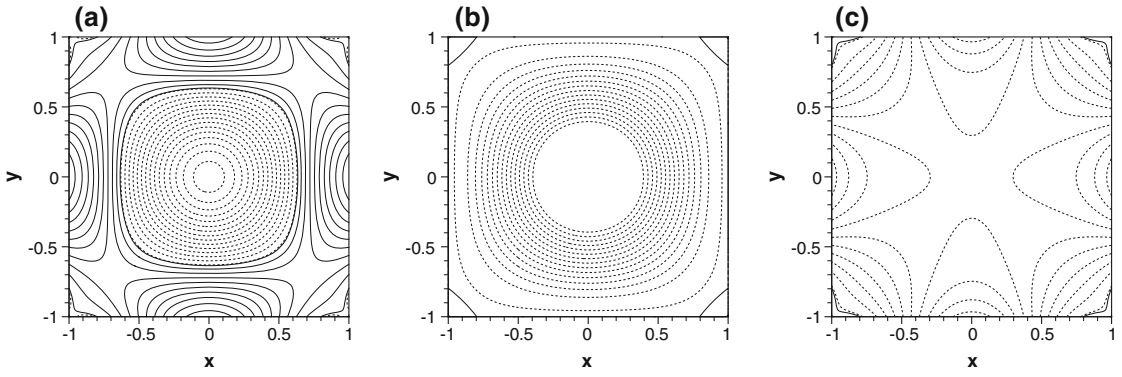

Fig. 4 **a** $\left(-\frac{\nu}{\lambda}\right)\omega(x, y)$, **b** $\psi(x, y)$ and **c** $\frac{\Pi(x,y)}{(-\lambda)}$, for the fundamental ($E1$, $\lambda/\nu = -13.086172791$) eigenmode in the square. The 26 contours correspond to values uniformly distributed between -0.01 and 0.007 at steps of 7.1×10^{-4}. *Solid* and *dashed lines* correspond, respectively, to positive (and zero) and negative levels

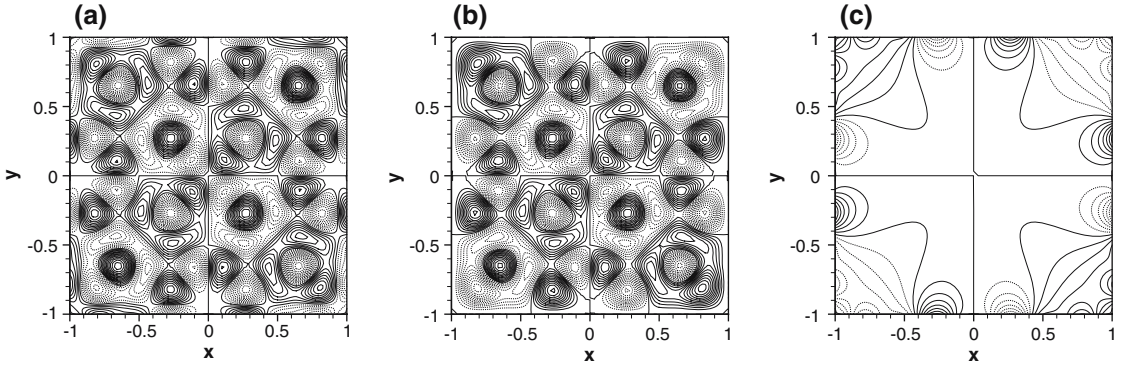

Fig. 5 **a** $\left(-\frac{\nu}{\lambda}\right)\omega(x, y)$, **b** $\psi(x, y)$ and **c** $\frac{\Pi(x,y)}{(-\lambda)}$, for the ($E2$, $\lambda/\nu = -331.966266$) eigenmode in the square. The 25 contours correspond to values uniformly distributed between -0.002 and 0.002 at steps of 1.67×10^{-4}. *Solid* and *dashed lines* correspond, respectively, to positive (and zero) and negative levels

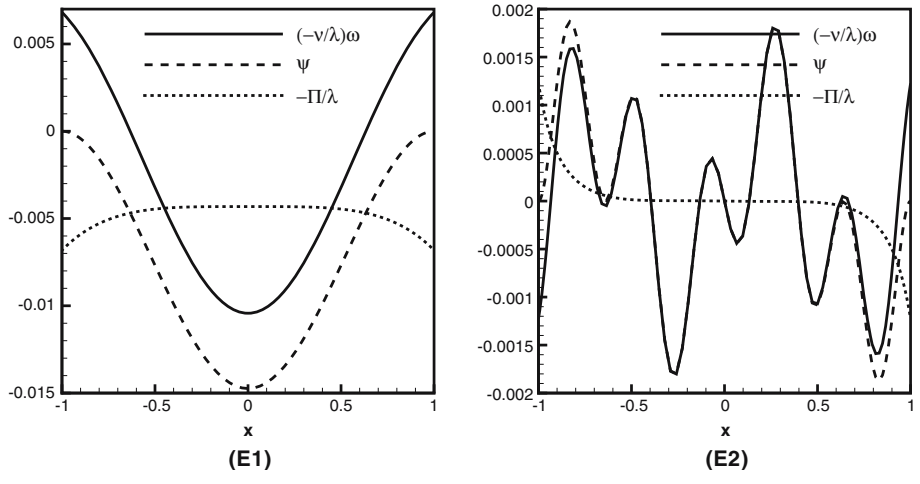

Fig. 6 The functions $\left(-\frac{\nu}{\lambda}\right)\omega(x, y = y_0)$, $\psi(x, y = y_0)$ and $\frac{\Pi(x,y=y_0)}{(-\lambda)}$, with $y_0 = 0$ for ($E1$, $\lambda/\nu = -13.086172791$) and $y_0 = -0.259$ for ($E2$, $\lambda/\nu = -331.966266$)

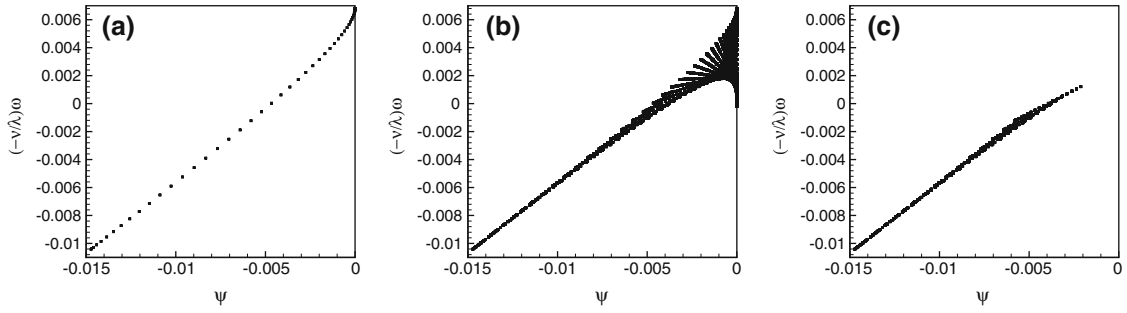

Fig. 7 Scatter plot of values of $\left(-\frac{\nu}{\lambda}\right)\omega(x, y)$ and $\psi(x, y)$ for the $(E1, \lambda/\nu = -13.086172791)$ eigenmode in the square; **a** along the cut at $y = y_0$, **b** in the whole square, **c** in the internal part of the square, $\mathcal{R}_C = (x, y) \in [-0.6, 0.6]^2$

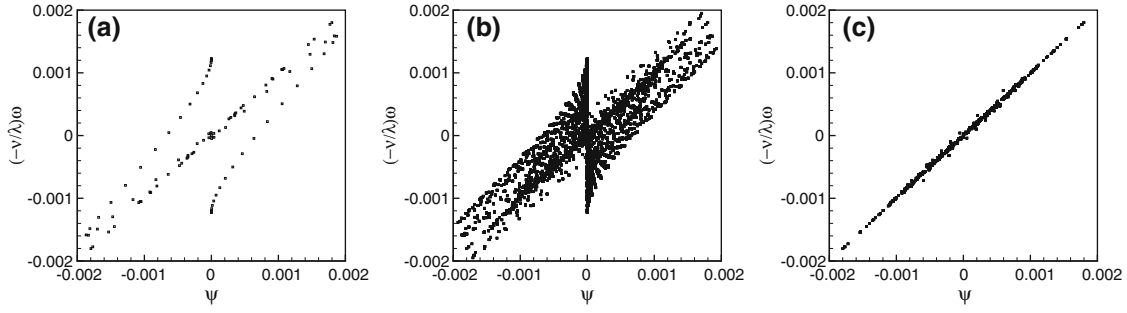

Fig. 8 Scatter plot of values of $\left(-\frac{\nu}{\lambda}\right)\omega(x, y)$ and $\psi(x, y)$ for the $(E2, \lambda/\nu = -331.966266)$ eigenmode in the square; **a** along the cut at $y = y_0$, **b** in the whole square, **c** in the internal part of the square, $\mathcal{R}_C = (x, y) \in [-0.6, 0.6]^2$

generates arcs on the $(\psi,\ \omega)$ correlation scatter plot [chart (a) of Fig. 8]. It is now easy to understand the origin of the butterfly shape of the $(\psi,\ \omega)$ correlation scatter plots published in [15,16], and shown in charts (b) of Figs. 7 and 8. The correlations that come from the $y = y_0$ lines are indeed simply reproduced after modulation by a function of y, and the wings generated in this way are bordered by the $\psi(x, y) = 0$ points associated with a given range of values of $\omega(x, y)$. A large part of these wings can be suppressed if the correlation is only taken with internal nodal values, where the $\frac{\Pi(x,y)}{(-\lambda)}$ amplitude becomes negligible. In charts (c) of Figs. 7 and 8, restricting the domain to $\mathcal{R}_C = (x, y) \in [-0.6, 0.6]^2$ leads to the almost linear $(\psi,\ \omega)$ relationships quoted in [9]. These relationships have the general expression

$$\nu\ (\omega - \omega_0) = -\lambda\,\psi,$$

where the offset ω_0 is only numerically measurable, provided the data are accurate enough. This offset cancels exactly for given symmetry properties, as with $E2$ according to Fig. 6.

4.4 The Stokes eigenmodes in the cube

Computing the Stokes eigenmodes in the cube is not an easy task, nor is the assessment of their physical relevance. Preliminary data regarding their computation can be found in [11]. Three components are here to be considered for the: the vorticity, $\vec{\omega}$, and vector potentials, $\vec{\psi}$ and $\vec{\Pi}$. Since these eigenmodes enjoy various symmetry properties, like those in the square [9], the $(\vec{\psi}, \vec{\omega})$ correlation can be presented equivalently with any of its three components. It is therefore chosen to consider only the x-component of this correlation for one eigenmode $(\lambda/\nu = -45.366354)$ computed with the PrDi numerical scheme [9] using 65^3 Chebyshev Gauss–Lobatto nodes.

Figure 9 shows a 3D plot of the fields $\left(-\frac{\nu}{\lambda}\right)\omega_x(x, y, z)$, $\psi_x(x, y, z)$ and $\frac{\Pi_x(x,y,z)}{(-\lambda)}$ where the surfaces of values $\pm 2.5 \times 10^{-4}$ and $\pm 5 \times 10^{-4}$ are represented. The extreme absolute value, 8×10^{-4}, occurs as a boundary value of the $\left(-\frac{\nu}{\lambda}\right)\omega_x$ and $\frac{\Pi_x}{(-\lambda)}$ fields. The similarity between the $\left(-\frac{\nu}{\lambda}\right)\omega_x(x, y, z)$ and $\psi_x(x, y, z)$ internal

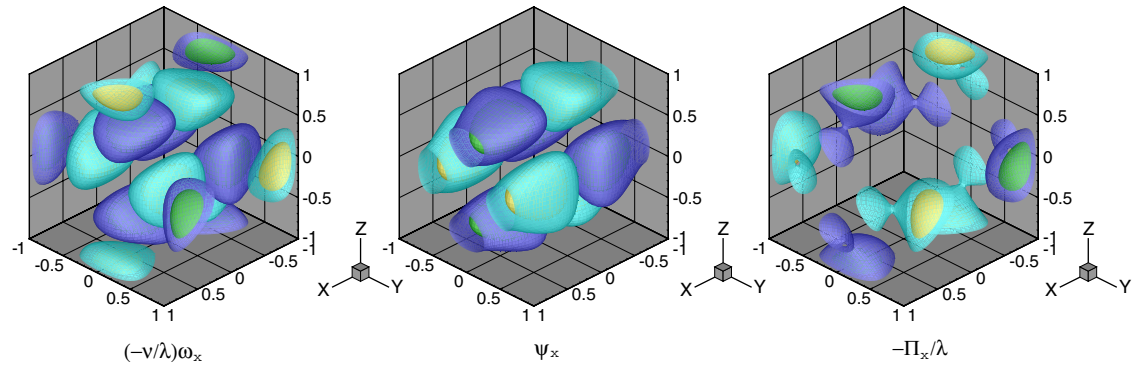

Fig. 9 $\left(-\frac{\nu}{\lambda}\right)\omega_x(x,y,z)$, $\psi_x(x,y,z)$ and $\frac{\Pi_x(x,y,z)}{(-\lambda)}$ for the $\lambda/\nu = -45.366354$ eigenmode in the cube. Four surfaces are represented, corresponding to the values -5×10^{-4} (*green*), -2.5×10^{-4} (*blue*), 2.5×10^{-4} (*cyan*), and 5×10^{-4} (*yellow*)[1]

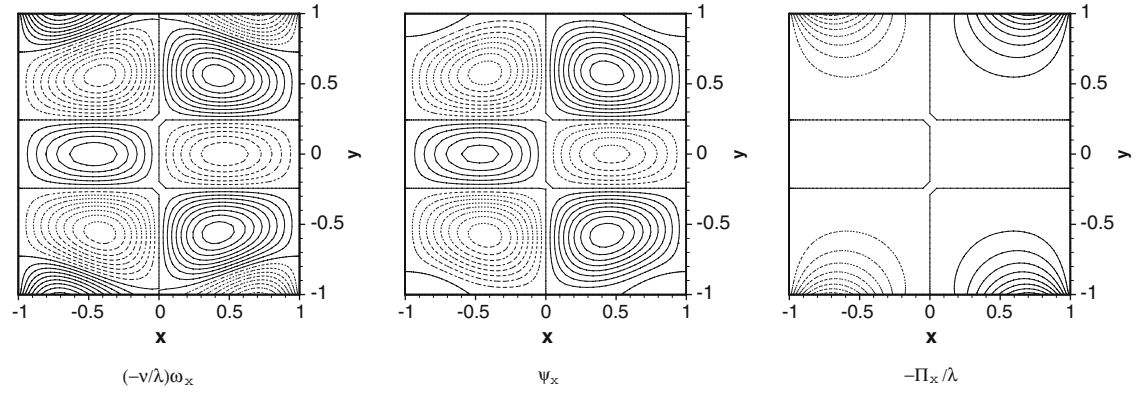

Fig. 10 Cross sections, at $z_0 = 0.243$, $\left(-\frac{\nu}{\lambda}\right)\omega_x(x,y,z=z_0)$, $\psi_x(x,y,z=z_0)$ and $\frac{\Pi_x(x,y,z=z_0)}{(-\lambda)}$, for the $\lambda/\nu = -45.366354$ eigenmode in the cube. The 25 contours correspond to values uniformly distributed between -0.001 and 0.001 at steps of 8.33×10^{-5}. *Solid* and *dashed lines* respectively correspond to positive (and zero) and negative levels

structures is clearly observable, as are their differences which mainly occur near the walls and correspond to the significant contribution of the $\frac{\Pi_x(x,y,z)}{(-\lambda)}$ field. This field becomes negligible with respect to the scale of both the others in the internal part of the cube, as shown in Fig. 10 where cross sections at $z_0 = 0.243$, $\left(-\frac{\nu}{\lambda}\right)\omega_x(x,y,z=z_0)$, $\psi_x(x,y,z=z_0)$ and $\frac{\Pi_x(x,y,z=z_0)}{(-\lambda)}$ are presented with the same scales and levels. The qualitative features exhibited by these plots are similar to those of Figs. 4 and 5, in particular in terms of the confinement near the boundary of the dominant $\frac{\Pi}{(-\lambda)}$ values.

Figure 11 shows the scatter plots of the correlations of $\left(-\frac{\nu}{\lambda}\right)\omega_x(x,y,z)$ versus $\psi_x(x,y,z)$, in the whole cube [plot (a)] and in two slightly different core domains $\mathcal{R}_C$, namely $\mathcal{R}_C = [-0.5967, +0.5967]^3$ in plot **(b)** and $\mathcal{R}_C = [-0.5556, +0.5556]^3$ in plot **(c)**.

The behaviors of these correlations are quite similar to those of the square case, in particular comparing the plots (b) and (c) of Fig. 8 respectively with plots (a) and (b), (c) of Fig. 11. The *butterfly* shape again comes out, firstly, with a vertical line at $\psi_x = 0$ and $\left|\left(-\frac{\nu}{\lambda}\right)\omega_x\right| \leq 8\times10^{-4}$, associated with the zeroes of ψ_x, its boundary values and its internal zeroes, and, secondly, with a thick horizontal zone about $\omega_x = 0$. The respective vertical and horizontal extensions of these line and zone give the exact Π_x (that is $\vec{\Pi}$) amplitude that is located on the boundary and in its neighborhood, as observed on chart (c) of Fig. 9. The *butterfly wings* together with a major part of these line and zone disappear when the correlation is taken in the internal part of the cube. The $(\vec{\psi},\ \vec{\omega})$ correlation then tends toward the approximate linear relationship:

$$\nu\ (\vec{\omega} - \vec{\omega}_0) = -\lambda\,\vec{\psi},$$

[1] The color version of this figure can be found in the online version at http://dx.doi.org/10.1007/s00162-006-0037-7

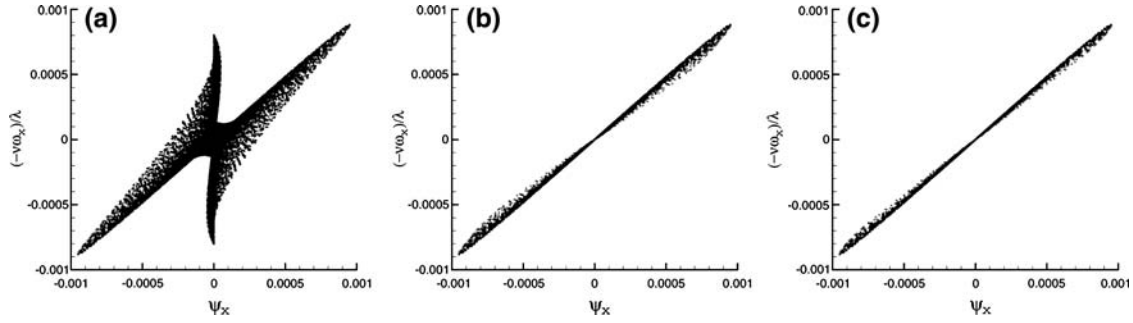

Fig. 11 Scatter plot of $\left(-\frac{\nu}{\lambda}\right)\omega_x(x, y, z)$ versus $\psi_x(x, y, z)$, for the $\lambda/\nu = -45.366354$ eigenmode in the cube. Plots **a**, **b** and **c** respectively come from the whole cube $[-1, +1]^3$, from $\mathcal{R}_C = [-0.5967, +0.5967]^3$ and from $\mathcal{R}_C = [-0.5556, +0.5556]^3$

where, again, the offset $\vec{\omega}_0$ is only numerically measurable, unless fixed to be exactly zero by symmetry considerations.

Plots (b) and (c) of Fig. 11 allow one to gauge the sensitivity of this relationship to the definition of $\mathcal{R}_C$. Reducing its extension on both sides by 0.04 in each space direction leads to narrower linear scatter plots.

4.5 Generalizing to the Stokes eigenmodes in any closed 2D/3D domain

From these particular cases, a general conclusion clearly emerges, already announced by the analysis of the dynamics made for the eigenmodes in the square (see paragraph 8.2.2 in [9]).

The key point is that the pressure is harmonic, $\vec{\nabla}^2 p = 0$, a property shared with the field $\vec{\Pi}$. In the case of the fully periodic Stokes eigenmodes (Sect. 4.1), this demands that the pressure gradient be exactly zero everywhere, since the spatial periodicity is realized in all directions.

When no-slip boundary conditions are imposed on the velocity over a boundary of any shape, a quasi-periodic pattern occurs for $\vec{\omega}$ and $\vec{\psi}$ along the boundary, a pattern which becomes increasingly periodic, in all space directions, as one moves into the domain. Accordingly, the vector potential $\vec{\Pi}$, the presence of which serves to compensate for the vorticity on the boundary, has the same quasi-periodic pattern on the boundary and therefore has to decrease towards some small value (possibly zero by symmetry) as one moves into the domain.

5 Conclusion

The general $(\vec{\psi}, \vec{\omega})$ correlation characterizing any unsteady harmonic-pressure viscous flow is given by the exact relation

$$\frac{\partial \vec{\psi}}{\partial t} + \nu\,\vec{\omega} + \vec{\Pi} = 0,$$

where the field $\vec{\Pi}$ is the pressure-gradient vector potential defined by

$$\vec{\nabla}\left(\frac{p}{\rho}\right) = \vec{\nabla} \times \vec{\Pi}.$$

Applied to the Stokes eigenmodes, of (real and negative) eigenvalue λ, satisfying no-slip boundary condition on the closure $\partial\Omega$ of any open domain Ω, this relation becomes

$$\lambda\,\vec{\psi} + \nu\,\vec{\omega} + \vec{\Pi} = 0\,, \quad \text{everywhere in } \Omega \text{ and on } \partial\Omega.$$

The field $\vec{\Pi}$ evolves in a quasi-periodic way along the boundary in order to balance the $\vec{\omega}$ field through the arbitrarily imposed (zero) value of $\vec{\psi}$. As a consequence of its harmonicity, $\vec{\Pi}$ accordingly has to decrease in amplitude, as one moves into the internal part of Ω, toward some small (and possibly zero) value, $\vec{\Pi}_{\text{core}}$, in the

core of this domain. An asymptotic $(\vec{\psi},\ \vec{\omega})$ relationship then emerges that characterizes the dynamics of each Stokes eigenmode in the internal part of the domain. It reads

$$\nu\ (\vec{\omega} - \vec{\omega}_0) = -\lambda\ \vec{\psi},$$

where the offset $\vec{\omega}_0$ is given by $\nu\,\vec{\omega}_0 = -\vec{\Pi}_{\text{core}}$.

6 Annex: brief survey of the eigenmode Chebyshev spectral solver

The Stokes eigenmodes in the squared and cubical domains were obtained by a Chebyshev spectral collocation solver dealing with the primitive variables formulation given by Eq. (6). The spatial discretization is based on the usual Chebyshev Gauss–Lobatto collocation method [4,6]. The velocity–pressure uncoupling is made by using the projection-diffusion (PrDi) algorithm ([3,8]). Section 3.2 in [8] provides all the details about the discrete PrDi scheme. This scheme is known to be consistent with the continuous uncoupled problem [8] and is one of the two solvers involved in the computation of the Stokes eigenmodes in the square [9,10] or in the cube [11]. The latter solvers, which are based on very different conceptual approaches to the PrDi method, were used to assess the results reliability and accuracy. Indeed, the Reid–Harris decomposition for the biharmonic stream-function problem and a lattice Boltzmann solver were implemented, respectively, for the square and cube cases.

The accuracy of the computed eigenvalues and eigenmodes has been documented in detail for the square case in [10]. For the cube configuration, the convergence of the eigenvalues with node number is reported in [11]. The 3D eigenmode that this paper uses in Sect. 4.4 has an eigenvalue determined with a relative error of about 2×10^{-6}, when going from a 33^3 to a 65^3 collocation grid.

Acknowledgements The second author gratefully acknowledges the financial support of the ERCOFTAC visitor program sponsored by the L. Euler Pilot Center (Switzerland) at EPFL. The computing resources were made available by the CSCS, Manno, Switzerland.

References

1. Batchelor, G.K.: On steady laminar flow with closed streamlines at large Reynolds number. J. Fluid Mech. **1**:177–190 (1956)
2. Batchelor, G.K.: An Introduction to Fluid Dynamics. Cambridge University Press, Cambridge (1967) (reprint 1994)
3. Batoul, A., Khallouf, H., Labrosse, G.: Une Méthode de Résolution Directe (Pseudo-Spectrale) du Problème de Stokes 2D/3D Instationnaire. Application à la Cavité Entrainée Carrée. C. R. Acad. Sci. Paris, **319**(I):1455–1461 (1994)
4. Canuto, C., Hussaini, M.Y., Quarteroni, A., Zang, T.A.: Spectral Methods in Fluid Dynamics. Springer Series in Computational Physics. Springer, Berlin Heidelberg New York (1988)
5. Constantin, P., Foias, C.: Navier–Stokes equations. Chicago Lectures in Mathematics. University of Chicago Press, Chicago (1988)
6. Gottlieb, D., Orszag, S.A.: Numerical Analysis of Spectral Methods: Theory and Applications. SIAM–CBMS, Philadelphia (1977)
7. Hirasaki, G.J., Hellums, J.D.: Boundary conditions on the vector and scalar potentials in viscous three-dimensional hydrodynamics. Q. Appl. Math. **XXVIII**(2):293–296 (1970)
8. Leriche, E., Labrosse, G.: High-order direct Stokes solvers with or without temporal splitting: numerical investigations of their comparative properties. SIAM J. Sci. Comput. **22**(4):1386–1410 (2000)
9. Leriche, E., Labrosse, G.: Stokes eigenmodes in square domain and the stream function–vorticity correlation. J. Comput. Phys. **200**(2):489–511 (2004)
10. Leriche, E., Labrosse, G.: Fundamental Stokes eigenmodes in the square: which expansion is more accurate, Chebyshev or Reid–Harris? Numer. Algorithms **38**(1,2):111–131 (2005)
11. Leriche, E., Lallemand, P., Labrosse, G.: Stokes eigenmodes in cubic domain: primitive variable and lattice Boltzmann formulations. Appl. Numer. Math. (2006) (in press)
12. Orszag, S.A., Israeli, M., Deville, M.: Boundary conditions for incompressible flows. J. Sci. Comput. **1**(1):75–111 (1986)
13. Taylor, G.I.: The Buckling load for a rectangular plate with four clamped edges. Ztschr. f. Angew. Math. Mech. **13**(2):147–152 (1933)
14. Temam, R.: Navier–Stokes equations: theory and numerical analysis. Studies in Mathematics and its Applications, vol. 2(3). North-Holland, Amsterdam (1984)
15. van de Konijnenberg, J.A.: Spin-up in non-axisymmetric containers. Ph.D. Thesis, Eindhoven University of Technology, 1995
16. van de Konijnenberg, J.A., Flor, J.B., van Heijst, G.J.F.: Decaying quasi-two-dimensional viscous flow on a square domain. Phys. Fluids **10**(3):595–606 (1998)
17. Yin, Z., Montgomery, D.C., Clercx, H.J.H.: Alternative statistical-mechanical descriptions of decaying two-dimensional turbulence in terms of "patches" and "points". Phys. Fluids **15**(7):1937–1953 (2003)